Impact of the annealing temperature on Pt/g-C_3N_4 structure, activity and selectivity between photodegradation and water splitting

Marine Caux [a], *Federica Fina* [a], *John TS Irvine* [a], *Hicham Idriss* [b], *Russell Howe* [c]

[a] *School of Chemistry, University of St Andrews, St Andrews, United Kingdom*

[b] *SABIC-Corporate Research and Development (CRD), KAUST, Thuwal, Saudi Arabia*

[c] *Chemistry Department, University of Aberdeen, Aberdeen, United Kingdom*

Corresponding author email address: mc253@st-andrews.ac.uk

ABSTRACT

This work presents a systematic study of the effect of fabrication temperature (450 to 650 °C) on the structure and electronic properties of g-C_3N_4 prepared from melamine. The work is conducted by X-ray diffraction, elemental analysis, BET nitrogen adsorption, UV-vis absorption, and electron paramagnetic resonance (EPR). The photocatalytic activity is tested for hydrogen production in the presence of oxalic acid (OA) as well as triethanolamine (TEOA). A considerable change in the morphology is observed with increasing the synthesis temperature resulting in an increase of the surface area, likely due to thermal etching at elevated temperatures. The decrease of charge carriers' concentration, per unit area, with annealing temperatures may be due to the decrease of the conjugation of the polymer. Probing the activity of g-C_3N_4 for hydrogen evolution reinforced this conclusion, the rate of hydrogen evolution per unit area for OA as well as TEOA decreased with annealing temperatures. An interesting finding is the correlation between CO_2:H_2 ratio and the increase in the band gap of g-C_3N_4 prepared at different temperatures when using oxalic acid as an electron donor. This suggests that water oxidation becomes easier with increasing band gap energy, probably due to a lowering of the valence band edge.

Key words:

photocatalysis, g-C_3N_4, synthesis temperature, hydrogen production, electron paramagnetic resonance

1. Introduction

Securing sustainable processes for energy production is an integral part for a future economy in order to curb atmospheric pollutions. Hydrogen production from water stemmed from the pioneering work of Fujishima and Honda [1] has attracted considerable attention of the scientific community. Hydrogen can be produced *via* either photo-degradation of organic compounds (i.e. photo-reforming for example) or direct water splitting. The latter is considered as the most challenging due to the thermodynamic limitation of the four holes process needed for water oxidation [2]. Hence one of the half reactions, usually proton reduction, is studied using sacrificial agents. Among the materials of recent interest are those based on g-C_3N_4 due to their stability and relatively small band gap (i.e. 2.7 eV) [3] when compared to other stable wide band gap materials.

Graphitic carbon nitride is a metal free semi-conductor composed mainly of carbon and nitrogen. The ideal g-C_3N_4 is composed of infinite and highly conjugated 2D sheets with a C/N ratio of 0.75 and a 3D organization close to graphite. Resolving the 2D structure has attracted a lot of attention and it has been shown that g-C_3N_4 is a tri-s-triazine unit based polymer [4]. More recently, the 3D organization of this highly disordered material has been investigated using X-ray diffraction and neutron scattering. The structure is best described by parallel chains of tri-s-triazine units organized in layers with a slight offset from each other in order to minimize the π-π interaction [5]. Unlike graphite, g-C_3N_4 is a semi-conductor due to the uniform distribution of the π electrons over the polymer network. The relatively small band gap of 2.7eV allows part of visible light harvesting, while its conduction band edge is well above the reduction potential of hydroxide ions to molecular hydrogen [3]. The valence band edge however is not ideally located with regards to the oxidation potential of water. The small energy difference suggests the need for a sacrificial agent in order to study the hydrogen evolution reaction [3].

Studies on the effect of the annealing temperature of g-C_3N_4 have previously been conducted by other workers [6–9] (among others), however few of those included EPR. Synthesis temperature affects the extent of the 2D ordering within the polymer and hence the number of defects present in the structure, which may be paramagnetic [10]. Studying the concentration of the paramagnetic charge carriers as a function of annealing temperature and the influence of band gap irradiation on these may bring new insight into the photocatalytic properties of g-C_3N_4.

In this work, we have studied the effect of synthesis temperature on g-C_3N_4 structure, BET surface area, band gap and charge carriers' concentrations in order to link them to the catalytic performance for hydrogen production. In particular, we would like to address the presence or absence of direct relationship between the surface area and photo-catalytic activity.

2. Experimental

2.1. Synthesis of Pt/g-C_3N_4 annealed at different temperatures

g-C_3N_4 was synthesized directly from melamine (99% Sigma Aldrich) via a solid state thermal polycondensation reaction procedure. The white precursor was heated at temperatures ranging from 450 to 650°C for 15 hours in static air (heating rate: 5°C·min^{-1}) in an alumina crucible covered with aluminum foil in order to minimize gas evolution. Platinum (1%wt) was loaded on the previously prepared g-C_3N_4 via an impregnation method from hexachloroplatinic acid ($H_2PtCl_6 \cdot 6H_2O$) (99.9% metal basis Alfa Aesar).

2.2. Characterisation

X-ray diffraction was carried out using a PANalytical Empyrean diffractometer equipped with a Cu radiation source. (i.e. CuKα1, $\lambda_{\alpha 1}$=1.5406 Å). Data were collected at room temperature.
A JASCO V650 spectrophotometer was used, for the absorbance of powdered samples, equipped with a 60 mm diameter integrating sphere (i.e. ISV-722) allowing diffuse reflectance measurements. Band gap determination was carried out via a Kubelka Munk transform, and Tauc plot using a dedicated software (i.e. SpectraManager, JASCO).
Paramagnetic centers on g-C_3N_4 were observed with a JEOL JES FA200 system- X band (i.e. 9 GHz) EPR spectrophotometer. The samples were loaded in high purity quartz cells then evacuated for 30 min to reach 10^{-6} mbar. Irradiation of the sample cavity was achieved using a 450W Xe lamp fitted with a narrow band pass filter (i.e. λ = 350-450nm).
A JEOL JSM-6700F Scanning Electron Microscope was used in secondary electron detection mode in order to analyze the morphology of the catalyst particles. The probe current and voltage used were: 5kV/10µA. Samples were gold coated with a Quorum Q150R ES gold sputter in order to decrease charging up.
Elemental analysis was performed using a Carlo Erba Flash 2000 Elemental Analyser. BET measurements were conducted on a Micromeritics TriStar II while an AccuPyc II 1340 pycnometer from Micromeritics was used for density measurements.

2.3. Photocatalytic testing for hydrogen evolution

The activity of the bare and platinum loaded g-C_3N_4 for hydrogen evolution was investigated using a custom designed reactor. In a typical run, 100 mg of catalyst were dispersed in 100 ml of distilled water (1g.L^{-1}) together with either oxalic acid (dihydrate ACS 99.5-102.5% Alfa Aesar) or triethanolamine (>99% Sigma Aldrich) as the sacrificial agent (respectively 0.025M, pH=1 and 10%vol: 0.753M, pH=10). The reaction was performed under inert atmosphere using argon. The reaction was performed in semi batch mode: sampling of the gas phase was performed every hour to allow H_2 and CO_2 evolutions to be monitored by gas chromatography (i.e. 3000 Micro GC from Agilent technologies; molecular sieve for H_2

and PLOT U for CO_2). Irradiation is carried out from the top using a 250V iron doped metal halide UV-vis lamp (i.e. 1000 mW/cm^2) equipped with a UV-cut off filter (i.e. allowing λ>380nm to irradiate the sample).

3. Results and discussion

3.1. Impact of the annealing temperature on g-C_3N_4 structure and morphology

X-ray diffraction patterns of the different materials are presented in Figure 1 A). The characteristic diffraction peaks at 2θ~ 13° and 27° can be observed on all patterns expect for CN450 which structure appears to be close to melem, known as an intermediate in the synthetic pathway of g-C_3N_4 [11]. The main diffraction peak at ca. 27° (d= ca. 3.2 Å) is attributed to the (002) plane and is due to distance *between* the 2D layers of the graphitic material [3], referred to here as $d_{2\ of\ (002)}$. The second peak located at 2θ = ca. 13° (d= ca. 6.7 Å) is due to the distance between the tri-s-triazine units *within* the 2D polymer frame [3], referred to here as $d_{1\ of\ (100)}$.

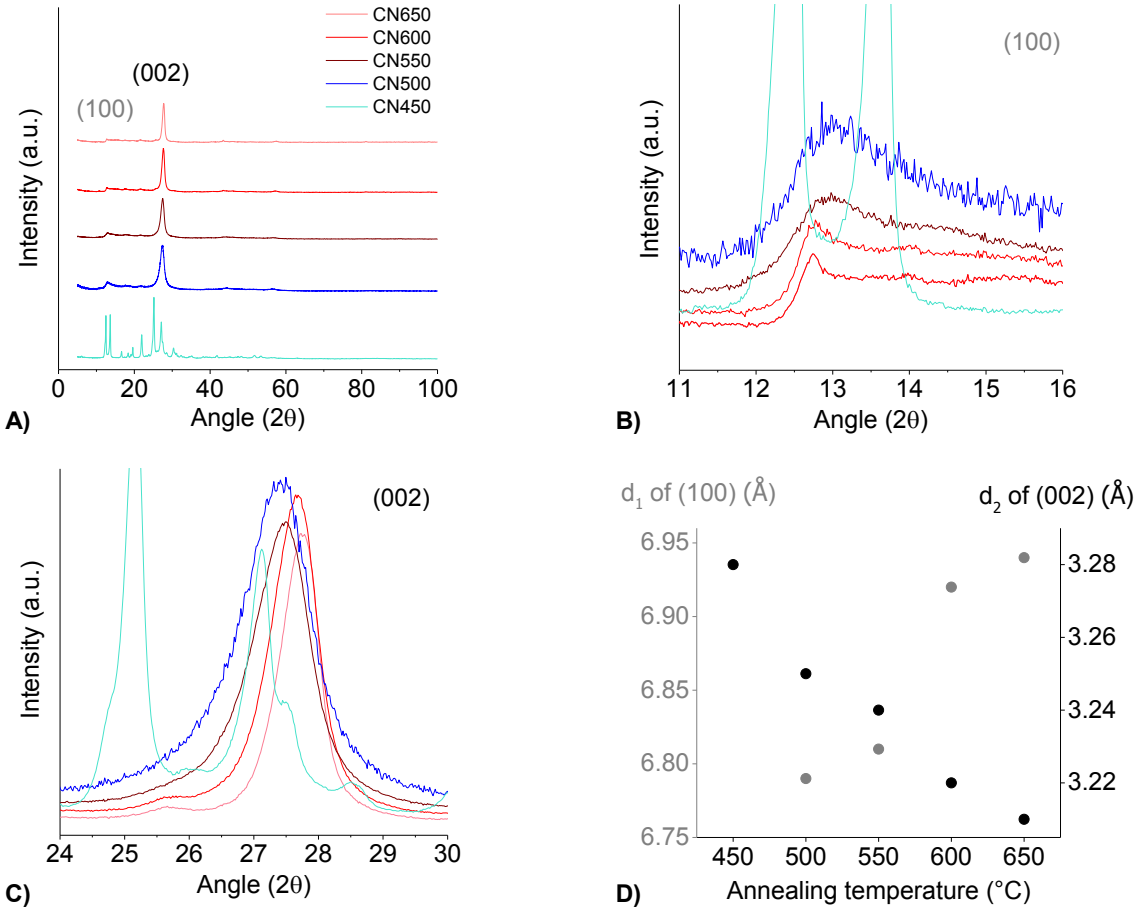

Figure 1: A) X-ray diffraction pattern of the g-C_3N_4 samples synthetized at different temperatures, B) and C) Zoom in of the XRD pattern for the main reflections $2\theta_1 \sim 13°$ and $2\theta_2 \sim 27°$ and D) Evolution of the d-spacing for (100) and (002) with annealing temperatures.

A narrowing of the two main diffraction peaks of g-C_3N_4 is observed when the synthesis temperature is increased. This indicates an increase in crystallinity; within the 2D layers as well as within the 3D packing of the polymer sheets. The d-spacing between the 2D layers of polymer ($d_{2\ of\ (002)}$) decreases when the annealing temperature of the material increases (see Figure 1 D)). This is supporting the higher crystallinity within the 3D organization of the material as this would bring a tighter packing of the polymer layers [8]. The opposite trend is observed for the spacing between the tri-s-triazine units ($d_{1of\ (100)}$), it increases with increasing annealing temperatures. This result could be explained either by a decrease of the conjugation on the tri-s-triazine units, due to the formation of defects or by a small shift of the tri-s-triazine unit layers stacked on top of each other.

The influence of synthesis temperature on the morphology of the different g-C_3N_4 was observed by SEM, as presented on Figure 2. Preparing the material at 450°C gives a monolithic morphology, the surface of the particles is smooth, and very few defects can be detected, similarly to Lotsch et *al.* [4]. When annealing the sample at 500 °C a clear layered structured appears hinting to the graphitic morphology of the bulk, observed in Figure 2 b).Then CN550 and CN600 show clear areas where the surface is very rough while retaining some smooth surfaces. When the sample is synthetized at 650 °C smooth surfaces are replaced by smaller particles giving it a rougher aspect.
A thermogravimetric analysis study conducted on the sample synthetized at 500 °C (see Figure S 1) shows that degradation starts between 500 and 550 °C. This may suggest that thermal decomposition leads to etching of the surface from 550 °C onwards removing the outer layer of material and revealing a particulate like morphology as observed on Figure 2 f) [7]. Upon comparison with a previous study it seems that when the synthesis is performed in an open system a similar effect can be observed on a much narrower range of temperatures [8].

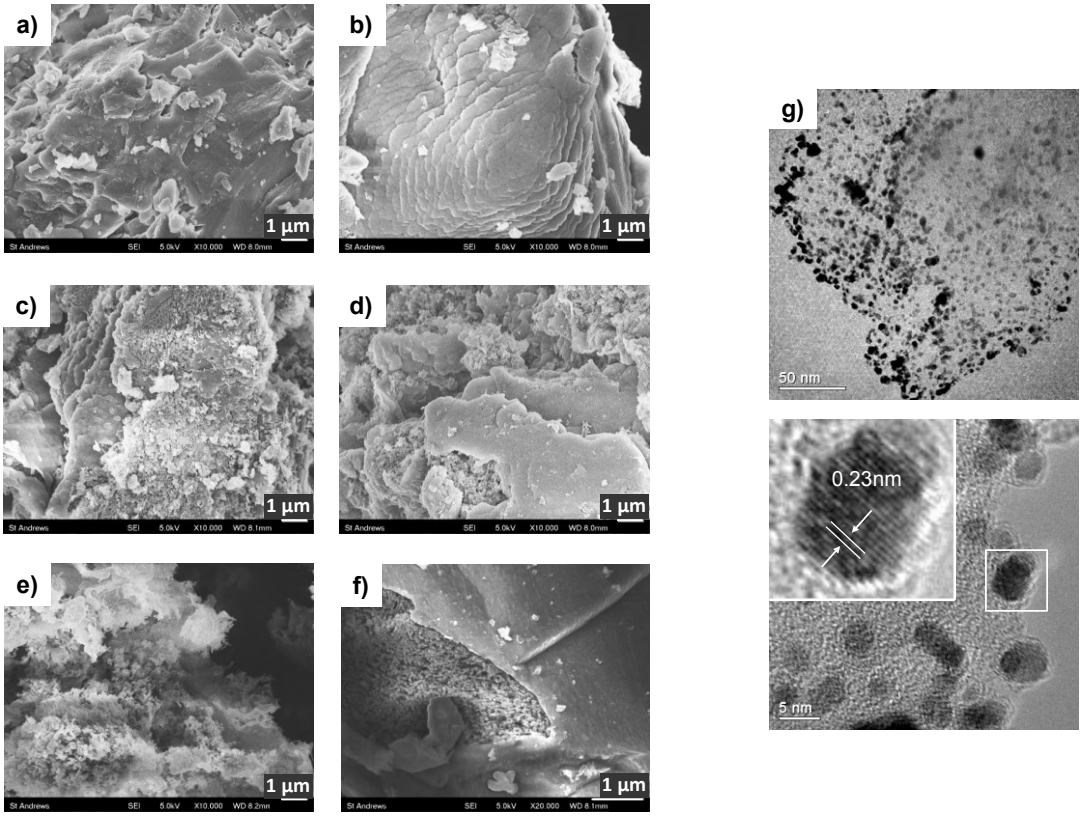

Figure 2: Scanning electron microscope (SEM) images of a) CN450, b) CN500, c) CN550, d) CN600, e) CN650 at a magnification of 10K, f) CN550 (represented in c) at 20K, and g) Transmission Electron Microscope (TEM) images of CN500 loaded with 1wt. %Pt after photocatalytic test using oxalic acid (0.025M) as sacrificial agent.

TEM micrographs on 1% wt. Pt loaded CN500 after photocatalytic tests are presented in Figure 2 g). Nanoparticles are observed on the micrographs with an average diameter of 5nm. The lattice fringes of 0.23nm are characteristics of Pt metal proving the in situ reduction of the chloroplatinic acid precursor [12]. XPS data presented in supplementary information (see Figure S 2) show the formation of platinum metal at the surface.

The surface area of the different samples as well as the apparent powder density and the absolute sample density are presented in Table 1. The low surface area characteristic of solid state synthesis increases with the annealing temperature from 4 to 41 $m^2.g^{-1}$. The apparent and absolute sample densities follow two opposite trends and are linearly correlated. When the annealing temperature increases, the absolute density increases while the apparent density decreases. This suggests that increasing the temperature during the synthesis of g-C_3N_4 leads to a denser sample as suggested by the tighter packing of the 2D layers of polymer along with higher inter-particle void. The latter is easily supported by the increased BET surface area and the rougher morphology displayed on the SEM images.

Table 1 : BET surface area (S_{BET}), absolute density (ρ), apparent powder density (ρ_a) and C/N, C/H, N/H ratios from elemental analysis for the different g-C_3N_4 prepared in this study.

	S_{BET} ($m^2.g^{-1}$)	ρ ($g.cm^{-3}$)	ρ_a ($g.cm^{-3}$)	C/N (atomic %)	C/H (atomic %)	N/H (atomic %)
CN450	4	1.71	0.35	0.63	1.86	1.16
CN500	10	1.80	0.31	0.67	2.41	1.60
CN550	22	1.90	0.27	0.68	2.75	1.86
CN600	38	2.16	0.16	0.68	3.45	2.35
CN650	41	2.39	0.09	0.68	3.88	2.65

Table 1 also shows elemental analysis data. The carbon to nitrogen ratio increased until 550°C, which is in line with the loss of NH_3 during the formation of melem and supported by the weight loss during the synthesis. However the C/N ratio plateaus at 0.68 which is quite far from the theoretical value of 0.75, suggesting residual N atoms on the edges of the polymer sheets. An increase of the carbon to hydrogen and nitrogen to hydrogen ratios was also observed which implies an increased number of tri-s-triazine units in the polymer layers of g-C_3N_4. This result is in line with the increased crystallinity within the 2D layers of polymer observed via XRD (see Figure 1).

3.2. Optical absorption and charge carriers' concentration of the g-C_3N_4 series

The UV-visible absorption in Figure 3 A) shows that all materials have a strong absorption around 400nm. The two samples synthetized at the highest temperatures are displaying an absorbance shoulder around 500nm, matching with their darker color [9]. The band gap of the different photo-catalysts were calculated using the Tauc plot for a direct allowed transition (n=1/2) [13]. Figure 3 B) shows that the band gap decreases when the synthetic temperature is increased up to 550 °C, in correlation with the C/N ratio. This is in line with previous findings on amorphous carbon doped with nitrogen suggesting that as the size of the sp^2 C=N clusters increases, the state density of π bonding in the sp^2 cluster increases leading to a decrease of the optical band gap [13–15]. It has to be noted that the material synthetized at 600 °C presents two different band gaps, which has not been reported in the literature so far [6,8,9,16].The lower one being in the continuity with the band gaps obtained for the materials synthesized at lower temperature while the higher one is closer to the data obtained at 650 °C. The synthesis temperature of 600 °C appears to be a turning point in the absorbance properties of g-C_3N_4.

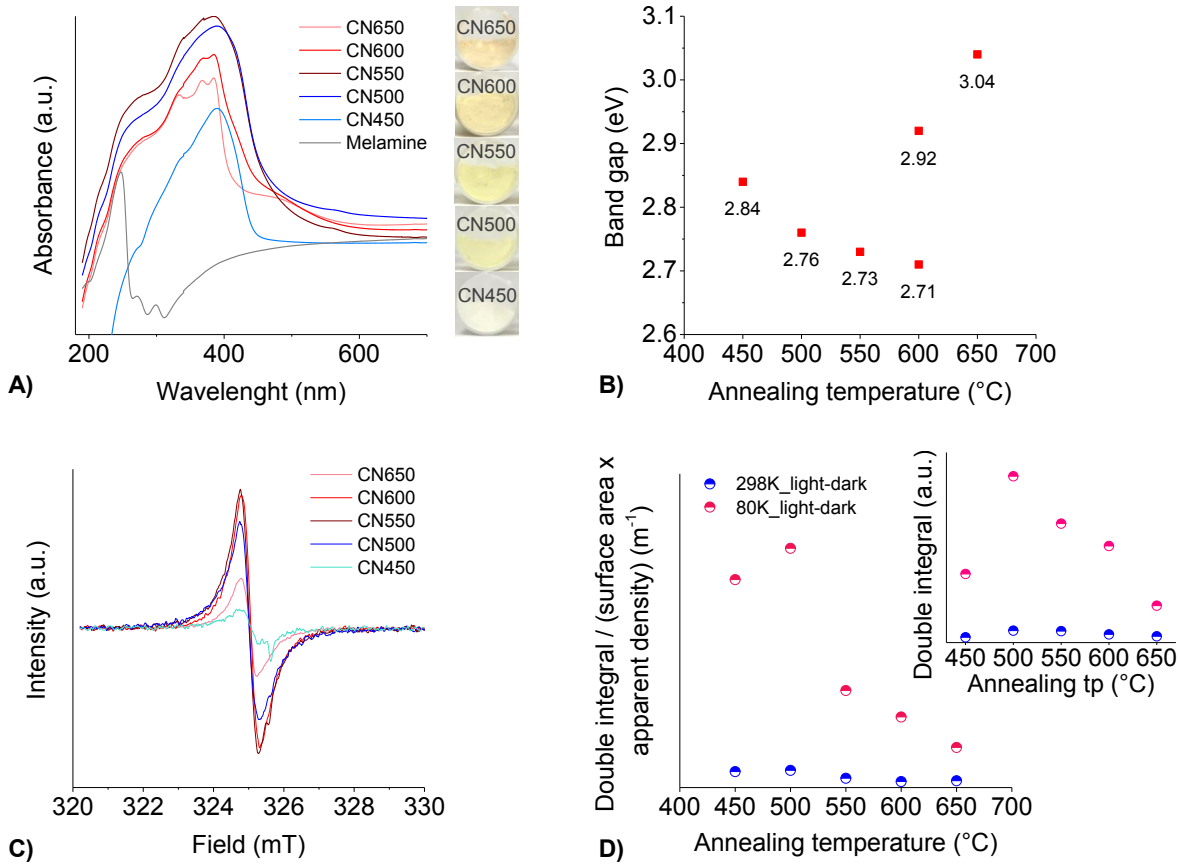

Figure 3 : A) UV-Vis Absorbance of the g-C_3N_4 series. B) Extracted direct band gaps of the g-C_3N_4 series. C) Lorentzian lines obtained by integration of electron paramagnetic resonance (EPR) absorption signal under 400nm light irradiation at room temperature. D) Doubly integrated EPR absorption signals under light irradiation at two different temperatures (80K and 298K), dark signal subtracted; data are normalized to the apparent density and the surface area of the samples.

Figure 3 C) presents the Lorentzian lines obtained during EPR data collection under light irradiation at room temperature. The absence of features in most of the signals obtained as well as the g value of 2.003 is coherent with previous literature findings. Most of the literature agrees that with such a g value and the absence of the typical hyperfine splitting expected from nitrogen; the EPR signal in carbon nitride polymers is likely to arise from unpaired electrons preferentially localized on carbon atoms [10,17,18]. However, a study based on solid state NMR and EPR shows that nitrogen located electron should not be ruled out, as electron delocalization could explain the absence of hyperfine splitting [19].

The sample synthetized at 450°C shows a small extra feature which can also be noticed in CN550 and CN500. As the crystallographic data suggested the sample synthetized at 450 °C is closer to melem than g-C_3N_4. Hence the extra line observed on those materials is most likely coming from some intermediate, as melem and melamine do not show any observable EPR signal [8]. As the apparent powder density and the surface area of g-C_3N_4 are impacted by the annealing temperature the EPR data has to be normalized to allow comparison of the samples between them. Moreover in order to monitor only the impact of light irradiation in the creation of paramagnetic centers, the signal obtained in the dark was subtracted.

The normalized doubly integrated EPR signal on Figure 3 D) shows that the increase of the signal under light irradiation is more dramatic at 80K than at 298K, however they both present almost the exact same trend. The concentration of paramagnetic species per volume and surface area increases from CN450 to CN500, where it reaches a maximum, and then decreases upon annealing at higher temperatures during the synthesis. EPR data under light irradiation is closely related to the separation of the charges formed due to light absorption. In graphitic carbon nitride charge delocalization over the π network is the key to charge separation, hence should be for photocatalytic activity. The sample synthetized at 450 °C stands out from the other ones showing an XRD pattern (see Figure 1 A)) close to melem, an intermediate in g-C_3N_4 polymerisation reaction. The increase in charge carriers' concentration from CN450 to CN500 is in line with a drastic change in crystalline structure revealing the fully polymerized material at 500°C. Then as the annealing temperature increases from 500 °C onward g-C_3N_4 gets more crystalline (see Figure 1 B) and C)). It is worth indicating that the surface of the photocatalyst increases together with an increase of $d_{1of(100)}$ (the d spacing between the tri-s-triazine units of the polymer) above 500°C (see Figure 2 and Figure 1 D)). The decrease in charge carriers' concentrations (see Figure 3 D)) may be linked to increasing amounts of surface or bulk defects formed upon annealing to higher temperatures as suggested by Gu *et al.* [8].

3.3. Effect of the sacrificial agent on photocatalytic hydrogen evolution and selectivity between water splitting and photodegradation

The photocatalytic activity of bare and 1%wt. platinum loaded g-C_3N_4 samples were tested in a custom made reactor using oxalic acid as a sacrificial reagent. Along with hydrogen, carbon dioxide was also monitored via gas chromatography as the result of oxidation of oxalic acid via the valence band holes of the semiconductor. Figure 4 A) shows the increase of activity when introducing a noble metal on the surface of g-C_3N_4 ; hydrogen evolution of g-C_3N_4 when synthetized at 450 °C increases from 54 to 3900 $\mu mol.h^{-1}g^{-1}$. Because Pt was present initially in both oxidized and reduced state, the induction period observed in the first few hours of the reaction is attributed to in situ reduction of the initially partially oxidized metal (see Figure S 3). XPS data and TEM micrographs supporting the presence of platinum in its reduced form after photocatalytic testing are presented in Figure S 2 and Figure 2 g). The positive impact of introducing platinum as co-catalyst has been reported numerous times on a various set of photocatalytic systems; it acts as an electron sink and therefore increases holes and electron separation [20,21], it is also thought to provide sites for H-H bond formation [22]. This same figure shows that the activity of the Pt/g-C_3N_4 catalyst decreases from 3900 $\mu mol.h^{-1}g^{-1}$ for CN450 to 1710 $\mu mol.h^{-1}g^{-1}$ for CN650. The trend observed for hydrogen evolution was similar to that of CO_2. Similar finding was made by Wu *et al.*; when using methanol as a sacrificial agent, they saw a clear decrease of the hydrogen evolution from 301$\mu mol.h^{-1}.g^{-1}$ at 520 °C to 59 $\mu mol.h^{-1}.g^{-1}$ at 640 °C [9]. Regarding our bare sample (see Figure 4 A) and B)) the activity seems to be maximal for CN500 (i.e. 125 $\mu mol.h^{-1}g^{-1}$) and decreases again at higher annealing temperature. A similar observation was made by Xu *et al* in 2013 on Eosin Y sensitized g-C_3N_4.

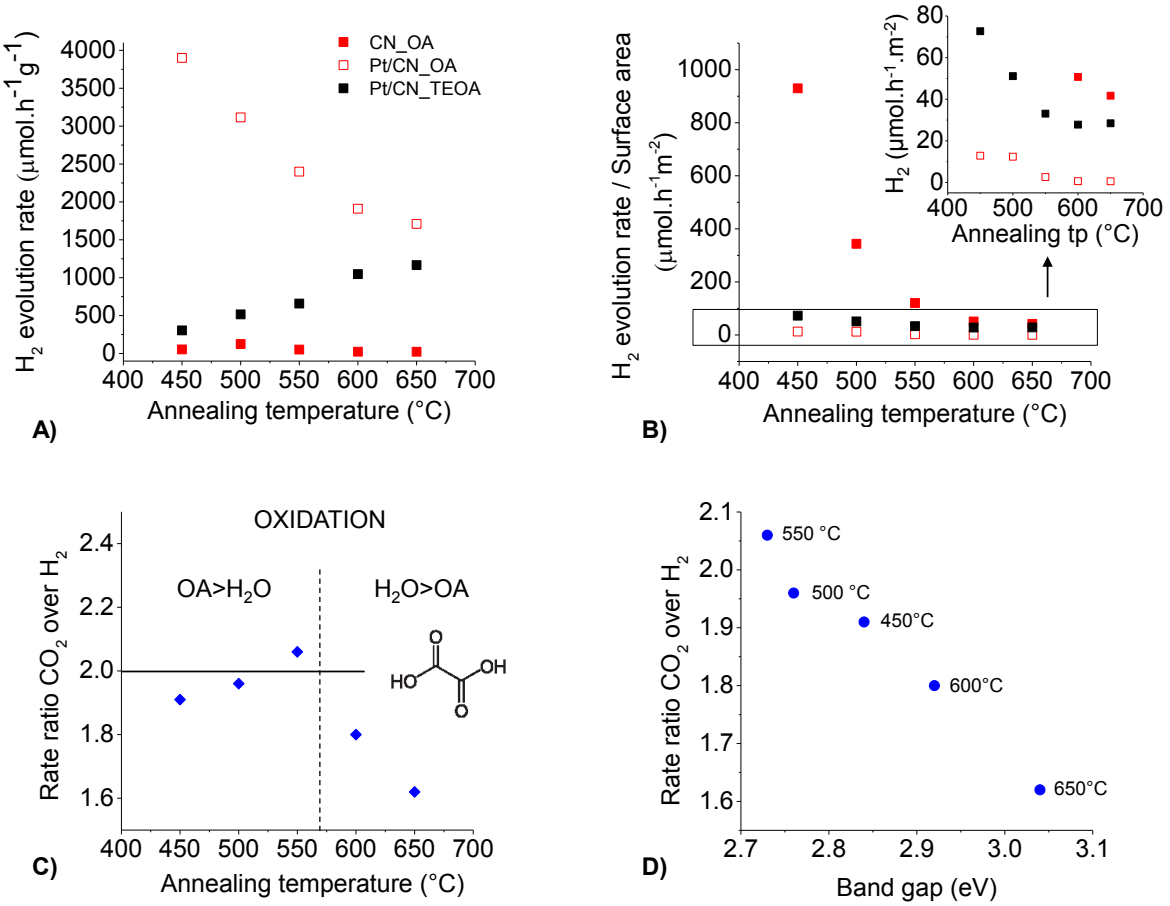

Figure 4 : A) Hydrogen production rate against prior annealing temperature of g-C_3N_4 bare or loaded with 1wt.% Pt, using oxalic acid (0.025M) or triethanolamine (10%vol) as sacrificial electron donor. B) Same rate as in A) normalized by surface area at each annealing temperature. C) Rate ratios between CO_2 and H_2 against the annealing temperature of g-C_3N_4. D) Rate ratio CO_2 and H_2 against the band gap of g-C_3N_4 synthetized at different temperatures.

An interesting finding was made when comparing the ratio between the rates of CO_2 and H_2. Figure 4 C) indicates that the ratio CO_2:H_2 increases from 1.91 at 450 °C to 2.06 at 550 °C then decreases down to 1.62 for CN650. Considering only photo-oxidation of oxalic acid, the theoretical ratio between hydrogen and carbon dioxide should be equal to 2. Hence, getting a ratio significantly lower of 1.8 and 1.62 for the two samples synthetized at the higher temperatures could suggest that oxidation of water is also taking place leading to a higher proportion of hydrogen being produced. Interestingly, the ratio between CO_2 and H_2 decreases when the band gap increases in a linear fashion as presented on Figure 4 D). Assuming that the conduction band edge is not affected by the annealing temperature as the band gap increases it is likely that the valence band is shifting to a more oxidizing energy level hence becomes better able to oxidize water. However, no significant oxygen evolution was detected to further confirm this theory. Photooxidation of water is known to be an inherently difficult process from a thermodynamic perspective [2,3]. There is growing evidence that water oxidation goes through the formation of surface hydrogen peroxide [23]. Evidence for the presence of hydrogen peroxide in solution after photocatalytic test with

oxalic acid as sacrificial agent has been found. However, at present more work is needed to optimize the analytic procedure before presenting quantitative data.
Hydrogen evolution was also probed using triethanolamine as a hole scavenger, at the exact same testing conditions. The rates of hydrogen production for each annealing temperature are presented in Figure 4 A). No carbon dioxide was detected this time, and the bare materials did not produce any observable hydrogen. Surprisingly, increasing the annealing temperature leads in this case to enhanced activity for hydrogen evolution. However, when normalizing the activity of the platinized g-C_3N_4 samples by the surface area of g-C_3N_4 in Figure 4 B), the hydrogen evolution per square meter of catalyst decreased with increasing the annealing temperature, similar to the case of oxalic acid albeit in alkaline pH.

Clearly, one should also consider that the disparity of Pt^0 nano particle size and dispersion might affect the hydrogen evolution. From Al-Azri et al. extensive study on the impact of metal particle size on hydrogen production, particle size does not seem to be a key variable [24]. On the other hand it was demonstrated that coverage is an important factor, with lower Pt coverages leading to better hydrogen evolution [12,25]. However the ratio Pt:PtO does not seem to affect the activity of 1%wt Pt/g-C_3N_4 [12]. In this work, each g-C_3N_4 sample was impregnated with 1%wt platinum and treated in the same way so it is reasonable to assume that the primary variable is the surface area of the catalyst, which in turn depends upon the initial thermal treatment.
The difference observed in terms of overall hydrogen evolution between TEOA (i.e. 51 $mmol.h^{-1}m^{-2}$) and OA (i.e. 343 $mmol.h^{-1}.m^{-2}$), for CN500, could be due to the difference of pH, hence to the concentration of proton in the solution [7]. Moreover, as the electron donors are quite different in terms of their chemical properties, it is likely that the mechanisms involved are not the same. Adsorption of TEOA as a rate determining step could further explain the positive correlation of hydrogen evolution with the surface area. The surface area gets larger at higher annealing temperatures which in turn would have been thought as leading to higher photocatalytic activity. However, electron paramagnetic resonance proved that the concentration of charge carriers (i.e. electron and/or holes) per square meter and per volume of sample decreased with increasing annealing temperatures, from 500 °C onwards. Hydrogen production rates observed in this study are in line with EPR results.

4. Conclusions

Graphitic carbon nitride synthetized at temperature ranging from 450 and 650 °C in a semi closed system was studied for its performance for hydrogen production. Increasing the synthesis (i.e. annealing) temperature resulted in: (i) increasing the surface area, (ii) increasing surface roughness and (iii) decreasing of the concentration of charge carriers per unit area. The destruction of the extensively conjugated system, key to electron/hole separation, from 500 °C onwards is a likely explanation for this trend [8]. Moreover, in order to assess the impact of the annealing temperature on the photocatalytic activity of g-C_3N_4 two different sacrificial agents were used: Triethanolamine (TEOA) and oxalic acid

(OA); the effect of which was studied. TEOA led to an increase of g-C_3N_4 activity per unit weight prepared at increased synthesis temperatures, while oxalic acid showed the opposite trend. However, normalizing the rate per unit area was found to give the same trend in both cases: a decrease with increasing the synthesis temperature. This is in line with the impact of synthetic temperature on the concentration of electrons and holes normalized by surface area. In addition, in the case of oxalic acid an excess of molecular hydrogen compared to the expected ratio between H_2 and CO_2 was obtained when g-C_3N_4 was synthetized at the higher temperatures (i.e. 600 and 650 °C). This surplus of hydrogen is likely coming from water oxidation in competition with oxalic acid oxidation. A linear correlation was obtained between the band gap and the ratio between hydrogen and carbon dioxide for the different annealing temperature suggesting that water oxidation may become easier when the band gap energy increases. Hydrogen peroxide as a reaction intermediate was detected in the post testing solution, however no solid conclusions can be drawn yet, work on progress.

Acknowledgements:

The authors would like to thank SABIC as well as EPSRC platform grant [EP/K015540/1] for financial support and the Royal Society of Chemistry for a Wolfson Merit Award.

REFERENCES:

[1] A. Fujishima, K. Honda, Nature. 238 (1972) 37–38.

[2] J. Tang, J.R. Durrant, D.R. Klug, J. Am. Chem. Soc. 130 (2008) 13885–91.

[3] K. Domen, X. Wang, K. Maeda, A. Thomas, K. Takanabe, G. Xin, J.M. Carlsson, M. Antonietti, Nat. Mater. 8 (2009) 76–80.

[4] B. V Lotsch, M. Döblinger, J. Sehnert, L. Seyfarth, J. Senker, O. Oeckler, W. Schnick, Chemistry. 13 (2007) 4969–4980.

[5] F. Fina, S.K. Callear, G.M. Carins, J.T.S. Irvine, Chem. Mater. 27 (2015) 2612–2618.

[6] J. Xu, Y. Li, S. Peng, G. Lu, S. Li, Phys. Chem. Chem. Phys. 15 (2013) 7657–7665.

[7] F. Fina, St Andrews university, 2014.

[8] Q. Gu, Z. Gao, H. Zhao, Z. Lou, C. Xue, RSC Adv. 5 (2015) 49317–49325.

[9] P. Wu, J. Wang, J. Zhao, L. Guo, F.E. Osterloh, J. Mater. Chem. A. 2 (2014) 20338–20344.

[10] D. Hollmann, M. Karnahl, S. Tschierlei, K. Kailasam, M. Schneider, J. Radnik, K. Grabow, U. Bentrup, H. Junge, M. Beller, S. Lochbrunner, A. Thomas, A. Bruckner, Chem. Mater. 26 (2014) 1727–1733.

[11] B. Jurgens, E. Irran, J. Senker, P. Kroll, H. Muller, W. Schnick, J. Am. Chem. Soc. 125 (2003) 10288–10300.

[12] F. Fina, H. Menard, J.T.S. Irvine, Phys. Chem. Chem. Phys. 17 (2015) 13929–13936.

[13] Y. Iwano, T. Kittaka, H. Tabuchi, M. Soukawa, S. Kunitsugu, K. Takarabe, K. Itoh, Jpn. J. Appl. Phys. 47 (2008) 7842–7844.

[14] J.R. Shi, Y.J. Xu, J. Zhang, Thin Film Solids. 483 (2005) 169–174.

[15] J. Robertson, Diam. Relat. Mater. 4 (1995) 297–301.

[16] S. Zuluaga, L.-H. Liu, N. Shafiq, S.M. Rupich, J.-F. Veyan, Y.J. Chabal, T. Thonhauser, Phys. Chem. Chem. Phys. 17 (2014) 957–962.

[17] J. Zhang, G. Zhang, X. Chen, S. Lin, L. Möhlmann, G. Dołęga, G. Lipner, M. Antonietti, S. Blechert, X. Wang, Angew. Chemie - Int. Ed. 51 (2012) 3183–3187.

[18] M. Tabbal, T. Christidis, S. Isber, P. Ḿrel, M. a. El Khakani, M. Chaker, A. Amassian, L. Martinu, J. Appl. Phys. 98 (2005) 044310–044310-8.

[19] D. Rovnyak, M. Baldus, B.A. Itin, M. Bennati, A. Stevens, R.G. Griffin, J. Phys. Chem. B. 104 (2000) 9817–9822.

[20] J. Yang, H. Yan, X. Zong, F. Wen, M. Liu, C. Li, Philos. Trans. R. Soc. London A Math. Phys. Eng. Sci. 371 (2013) 20110430.

[21] J. Yang, D. Wang, H. Han, C. Li, Acc. Chem. Res. 46 (2013) 1900–1909.

[22] M.A. Fox, M.T. Dulay, Chem. Rev. 93 (1993) 341–357.

[23] J. Liu, Y. Liu, N. Liu, Y. Han, X. Zhang, H. Huang, Y. Lifshitz, S. Lee, J. Zhong, Z. Kang, Science. 347 (2015) 970–974.

[24] Z.H.N. Al-Azri, W.-T. Chen, A. Chan, V. Jovic, T. Ina, H. Idriss, G.I.N. Waterhouse, J. Catal. 329 (2015) 355–367.

[25] H. Courbon, J. Herrmann, P. Pichat, J. Phys. Chem. 88 (1984) 5210–5214.